DOI: 10.1002/ejic.200901114

Surfactantless Synthesis and the Surface-Enhanced Raman Spectra and Catalytic Activity of Differently Shaped Silver Nanomaterials

Xuanhua Li,[a,b] Jin Wang,[a] Yongxing Zhang,[a,b] Mingqiang Li,[a] and Jinhuai Liu*[a]

Keywords: Silver / Nanostructures / Raman spectroscopy / Catalytic activity

This paper reports the transition of shape-selective silver nanostructures from nanoplates to nanodendrites and to nanospheres made up of primary nanoparticles that can be readily controlled by changing the molar ratio of vitamin C to $AgNO_3$. In addition, the formation of Ag nanostructures with multiple shapes can be readily controlled depending on the efficient density-assisted self-assembly synthesis. The surface-enhanced effects and catalytic activity of the formed Ag nanomaterials are strongly dependent on the surface morphologies of Ag nanomaterials, and compared with the other Ag nanomaterials presented here, the nanospheres made up of primary nanoparticles showed excellent surface-enhanced effects and catalytic activity.

Introduction

Currently, differently nanostructured Ag has attracted much interest due to its catalysis,[1] antibacterial activity,[2] unique optical properties, and ultrasensitivity, which makes Ag another promising candidate for chemo- or biosensing by surface-enhanced Raman spectra (SERS).[3–5] Furthermore, strong enhancement of the electromagnetic field near the surface of complex structures has been shown from experimental measurements[6] and theoretical calculations.[7] Hence, synthesis of nanomaterials with these complex structures has taken place recently.

Several principal strategies for generating these complex nanostructures (e.g., electrochemical synthesis,[8] oriented attachment,[9] the use of specific capping agents to induce anisotropic growth,[10] and so on) have been reported. However, reducing agents used in some of these approaches have been suggested to be harmful to the environment. Hence, the exploration of facile green synthetic routes for the self-assembly of nanostructured metal is important but challenging. Varma and co-workers have developed a microwave irradiation method to produce snowflake-like three-dimensional nanostructured metal oxides.[11] Although Varma and co-workers have reported the green synthesis of core–shell metallic nanocrystals using aqueous vitamin C,[12] and Xia and co-workers reported the synthesis of Ag nanodendrites using aqueous vitamin C,[13] they have not reported the synthesis of other shaped Ag nanostructures such as nanoplates, nanospheres, and so forth. Therefore, investigations on the fabrication of nanostructured metals with different shapes by the reduction of vitamin C without surfactant are still challenging. Compared to harmful reducing agents (e.g., sodium borohydride or hydroxylamine hydrochloride), vitamin C is a mild reducing agent with biodegradability and low toxicity. Consequently, it is considerably worthwhile for us to continue to study vitamin C as a reductant without introducing any template or surfactant, as reported in this present paper.

Recently, Bond and co-workers reported the synthesis of 1D silver nanowires and 3D silver clusters through a thermodynamic or a kinetic pathway, respectively.[14] Herein, we present a modified vitamin C reduction method to produce silver 2D and 3D nanostructures. We will show that by changing the molar ratio of vitamin C to $AgNO_3$ with a considerable range of about 800, a transition of shape-selective silver nanostructures from nanoplates to nanodendrites and to nanospheres made up of primary nanoparticles can be readily controlled. Furthermore, we have also controlled the synthesis of silver nanomaterials of various shapes depending on the density of the solvent, by which we can speculate on the silver nanostructured shape during the efficient density-assisted self-assembly synthesis. In addition, a potential application of the Ag nanomaterials as an SERS-active material has been probed with rhodamine 6G (R6G), and extensive applications toward catalyzing a redox reaction of 4-nitrophenol in the presence of the Ag nanomaterials are discussed in detail.

[a] The Key Laboratory of Biomimetic Sensing and Advanced Robot Technology,
Institute of Intelligent Machines, Chinese Academy of Sciences,
Anhui 230031, P. R. China
Fax: +86-551-5592420
E-mail: jhliu@iim.ac.cn
[b] School of Chemistry and Material Science,
University of Science and Technology of China,
Anhui 230026, P. R. China

Supporting information for this article is available on the WWW under http://dx.doi.org/10.1002/ejic.200901114.

Results and Discussion

The formation of nanoplates, nanodendrites, and nanoparticles occurred at room temperature. The addition of vitamin C to Ag salts resulted in a change in color (slight brown to yellow), thus indicating the formation of an Ag nanostructure. Depending upon the molar ratio of vitamin C to $AgNO_3$ used for the preparation, Ag crystallized in different shapes and sizes. For example, a lower molar ratio of vitamin C to $AgNO_3$ (Table 1, Ag-2 and Ag-10) yielded a platelike structure (Figure 1, A and B). The thickness of these plates varied from 20 to 80 nm with a length of about 500 nm to 1.5 μm. An increase in the molar ratio of vitamin C to $AgNO_3$ (Table 1, Ag-50) resulted in the formation of a crablike structure (Figure 1, C and D). The short rods were grown on the side face of a single Ag nanoplate mimicking the crablike structures.

Table 1. Synthesis of Ag nanoparticles.

Composition	Molar ratio[a]	Code
0.12 mL of VC + 1 mL of $AgNO_3$	2	Ag-2
0.6 mL of VC + 1 mL of $AgNO_3$	10	Ag-10
3 mL of VC + 1 mL of $AgNO_3$	50	Ag-50
6 mL of VC + 1 mL of $AgNO_3$	100	Ag-100
6 mL of VC + 0.5 mL of $AgNO_3$	200	Ag-200
6 mL of VC + 0.25 mL of $AgNO_3$	400	Ag-400
6 mL of VC + 0.125 mL of $AgNO_3$	800	Ag-800

[a] The molar ratio indicates the millimolar ratio of vitamin C (VC) to $AgNO_3$.

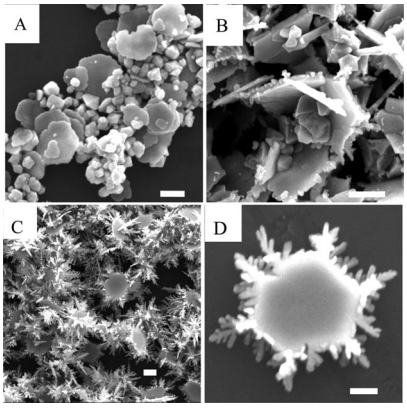

Figure 1. Field-emission scanning electron microscopy (FESEM) images of (A) Ag-2, (B) Ag-10, and (C, D) Ag-50. All scale bars are 500 nm.

Further continual increase in the molar ratio of vitamin C to $AgNO_3$ (Table 1, Ag-100, Ag-200, and Ag-400) started the growth of Ag dendrites. It can be observed that growth progresses from linear dendrites (Figure 2, A and B) towards the formation of many radial irregular dendritic stemlike structures with the length (around 50–350 nm) and diameter (below 100 nm) of a single dendrite (Figure 2, C and D).

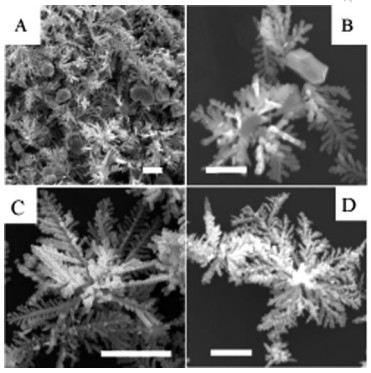

Figure 2. FESEM images of (A, B) Ag-100, (C) Ag-200, and (D) Ag-400. All scale bars are 500 nm.

It is worth mentioning here that there was a shift from the Ag nanodendrites to nanospheres made up of the primary nanoparticles (Figure 3, A and B) when the molar ratio of vitamin C to $AgNO_3$ increased to 800 (Table 1, Ag-800). As indicated by the arrows, there were some dendritic remnants mixing with the nanospheres. Every nanosphere had a large total surface area due to the agglomeration of primary Ag nanoparticles that led to the roughness of the surface of the nanospheres.

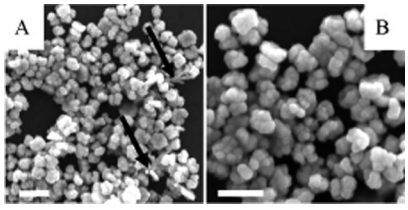

Figure 3. FESEM images of low and high magnifications of the Ag-800 sample. All scale bars are 500 nm.

The TEM images (Figure 4, A–G) show the changes of Ag nanomaterials from nanoplates to nanospheres made of primary nanoparticles accompanied by the gradual increase of the molar ratio of vitamin C to $AgNO_3$ from 2 to 800. As can clearly be seen, the Ag nanoplates (Figure 4, A) first shifted to crablike nanoplates (Figure 4, B) and to nanodendrites (Figure 4, C and D). After that, the nanodendrites made up of differently sized rods (Figure 4, C and D) changed to nanodendrites made up of small nanoparticles (Figure 4, E and F). Lastly, the nanomaterials were predominantly a majority of nanospheres made up of the primary nanoparticles (Figure 4, G). As indicated by the arrows, there were some nanoscale cavities between the primary nanoparticles on the nanospheres, which are potential "hot" spots for localized near-field enhancement effects.

The crystalline characteristics of the nanostructured silver with different shapes, including Ag-10, Ag-50, Ag-400, and Ag-800, were investigated by XRD (Figure 5, A). The peaks observed at 2θ = 38.2, 44.6, 64.2, and 77.1° can be respectively assigned as (111), (200), (220), and (311) lattice planes of face-centered cubic (FCC) metallic Ag (JCPDF card no. 04-0783). From the XRD pattern, it is clear that there is only one peak indexed as [111] to nanoplates (Ag-

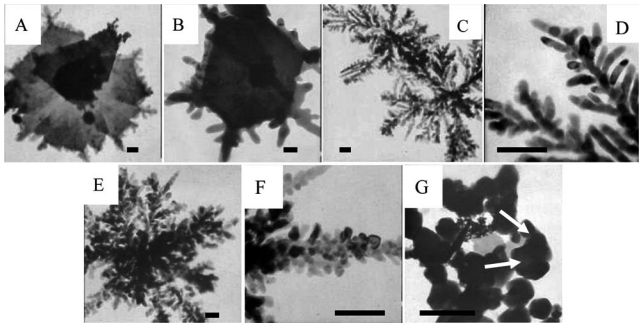

Figure 4. Representative TEM images of the Ag nanomaterials: (A) Ag-10, (B) Ag-50, (C, D) Ag-200, (E, F) Ag-400, and (G) Ag-800. All scale bars are 200 nm.

10) and mainly two peaks, [111] and [200], attributed to nanoplates with nanorods (Ag-50). Because the nanoplates are thin flakes and the {111} facets are almost the only ones parallel to the Si substrate, only the [111] peak appears in the XRD pattern.[15] According to the crystal-face growth rule put forward by Gilman, Brice et al., to reach the state of thermodynamic stability, the crystal faces with high free energies should grow more quickly and be more difficult to expose to a large degree.[16] However, the crystal faces with low free energies can be exposed to a large degree, such as the {111} crystal face. Thus the crystal faces with higher surface free energies, such as {110} and {311} crystal faces, should more easily appear on edges, corners, protuberances, and so on to a very small degree. It is reasonable that the as-prepared nanodendrites and nanoparticles should show all the crystal planes of FCC silver, such as the [200], [220], and [311] peaks; and with the change of shape from nanodendrites to nanospheres, the diffraction-peak ratios of the first peak to the second peak or to the third peak decrease gradually, probably because of their random polyhedron morphology.[17] All the results of XRD analysis agree well with the previous reports.[18,19]

It is of interest to explore optical properties of the Ag nanomaterials (Figure 5B). The nanospheres made up of primary nanoparticles (Ag-800) exhibit a plasmon peak at about 412 nm,[20] and the nanodendrites (Ag-400) show a broad plasmon peak from 410 to 600 nm.[21] The nanoplates (Ag-10) and the nanoplates with short rods (Ag-50) mainly have two peaks attributable to the weak out-of-plane quadrupole (about 335 nm) and in-plane dipole plasmon resonance (a wide absorption in the visible region from 400 to above 600 nm).[22]

Although the mechanism for the formation of nanostructures is not clear, we believe the molar ratio of vitamin C to $AgNO_3$ used in the preparation plays a key role in orchestrating the final structure of Ag nanostructures. At a lower molar ratio, there is more freedom for Ag embryos to promote a highly anisotropic growth in the two directions such as the <100> and <110> directions, thus extending into large nanoplates with [111] basal faces and ultimately leading to selective growth of the silver nanoplates because of lower reduction ratio and weaker protection.[23] On the contrary, at a high molar ratio, there is insufficient

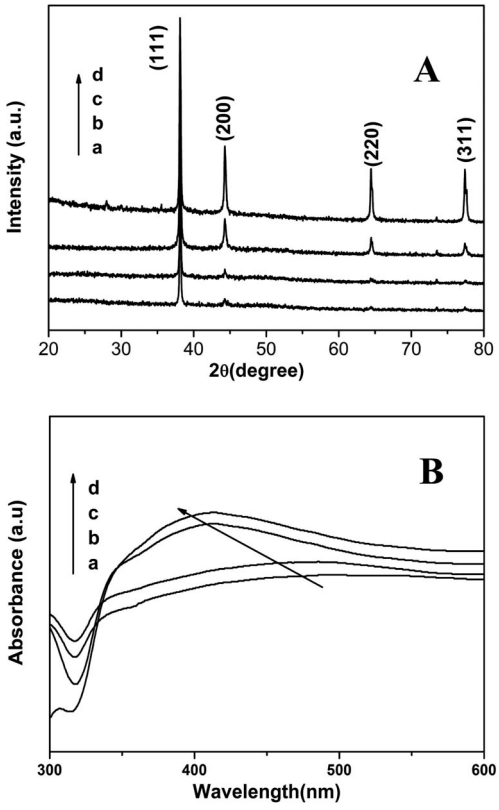

Figure 5. (A) XRD pattern of the samples: (a) Ag-10, (b) Ag-50, (c) Ag-400, and (d) Ag-800; (B) UV/Vis absorption spectra of samples: (a) Ag-10, (b) Ag-50, (c) Ag-400, and (d) Ag-800.

freedom for the crystals to agglomerate, and this strongly impacts on the proliferation of crystals because the quantity of capping agent shows a strong steric effect.[24,25] Generally speaking, the 2D growth pathway is attributed to thermodynamic control, whereas 3D growth is attributed to kinetic control.[14] Therefore, if we want to synthesise Ag nanoplates, we can control the reaction in the thermodynamic path by keeping the molar ratio of vitamin C to $AgNO_3$ below 10. On the contrary, by changing the molar ratio of vitamin C to $AgNO_3$ to more than 100, the reaction will follow the kinetic path and therefore nanodendrites can be synthesized effectively. With a molar ratio of vitamin C to $AgNO_3$ between approximately 10 to about 100, the reactions are controlled by both thermodynamics and kinetics, and crablike nanostructures can thus be attained.

We also investigated the effect of solution with varying densities on the shape of the Ag nanomaterials. Figure 6 depicts typical FESEM images of the Ag nanoparticles (Figure 6, A), the mix of nanoparticles and short rods (Figure 6, B), nanospheres made up of short rods (Figure 6, C), and the nanoflowers (Figure 6, D) in the different solutions: glycol (ρ = 1.113), water (ρ = 1.0), DMF (ρ = 0.9445), and isopropyl alcohol (IPA; ρ = 0.784) instead of methanol (ρ = 0.789), respectively. It has been found that the self-assembly of nanoparticles is determined by various factors such as surfactant concentration, ionic strength,[26] pH,[27] temperature,[28] and slow evaporation of the solvent;[29] and

according to one report,[30] solvent density plays a crucial role in governing the controlled growth of different self-assembled structures and shapes. The formation of Ag nanostructures with multiple shapes, depending on the density of the solvent used for the preparation, is shown in Figure 7. Clearly, with the decrease of density from 1.111 to 1.0 and to 0.945, the shape of the Ag nanomaterials changed from nanoparticles to a mix of nanoparticles and short nanorods, and to only short nanorods. Further reduction of the solvent density by using methanol and isopropyl alcohol in the preparation of Ag nanoparticles yielded nanodendrites with diameters of less than one micron. According to this rule, we can speculate on the shapes of the silver nanomaterials in some other solvents. For example, if we want to synthesize Ag nanoparticles and Ag dendrites, we can choose acetate (ρ = 1.048) and acetonitrile (ρ = 0.781) as solvents, respectively. In fact, the hypothetical results are consistent with the experimental results (see Figure S1 in the Supporting Information). Although the mechanism involved in how solvent density affects the shape of nanoparticles is not clear, we can be sure that the density of a solvent as a given instantaneous driving force is responsible for the self-assembly of Ag nanomaterials. This is due to the mobility of nanoparticles in a given solvent. All the results agree well with previous reports.[30]

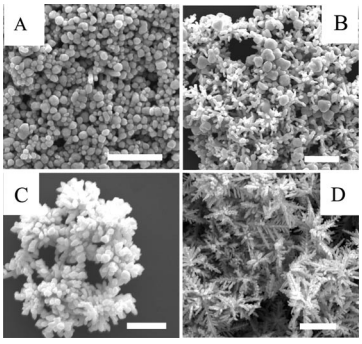

Figure 6. Representative FESEM images of the Ag nanomaterials synthesized using vitamin C in different solutions: (A) glycol, (B) water, (C) DMF, and (D) isopropyl alcohol. All scale bars are 1 μm.

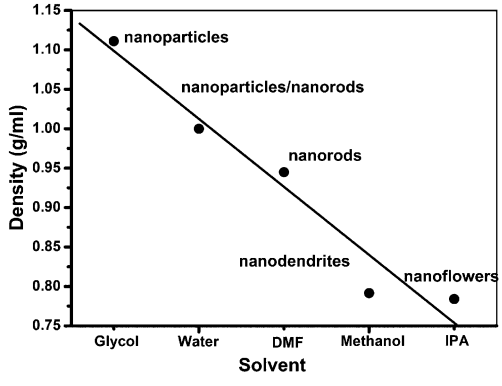

Figure 7. The formation of Ag nanostructures with multiple shapes depending on the density of the solvent used for the preparation.

As discussed above, nanomaterials with different shapes and sizes exhibit different SERS enhancement.[31] Figure 8A shows the SERS of R6G in the presence of different Ag nanomaterials. The peaks from 600 to 1800 cm^{-1} are attributed to R6G signals; vibrations at 1187, 1311, 1363, 1508, and 1650 cm^{-1} are assigned to C–H in-plane bending, C–O–C stretching, and C–C stretching of the aromatic ring;[32] and a low concentration of R6G produces a clear enhanced effect at 1650 cm^{-1}, which is one of the main characteristic bands.[5] In comparison with the SERS spectrum of Ag-10, Ag-50, and Ag-400, the magnitude of the signal from Ag-800 is much greater.

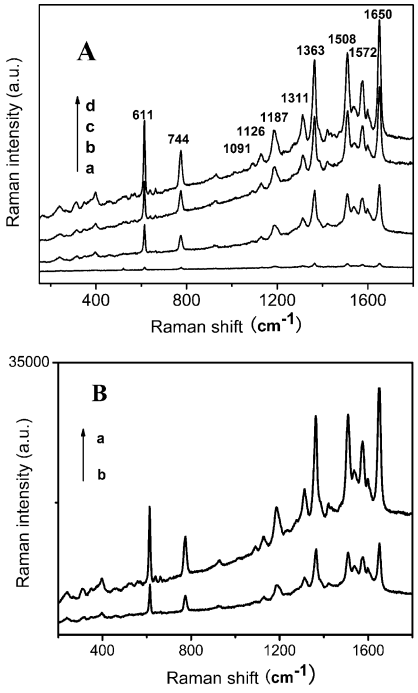

Figure 8. (A) SERS spectral comparison of R6G (10 nM) in the presence of (a) Ag-10, (b) Ag-50, (c) Ag-400, or (d) Ag-800. (B): SERS spectral comparison of R6G (10 nM) in the presence of (a) Ag-800 and (b) Ag nanoparticles with a smooth surface and a size of about 73 nm.

In addition, the formed Ag-800 was evaluated relative to the existing Ag nanoparticles. Previous studies have shown that Ag nanoparticles with a size of around 60–80 nm have the highest efficiency for SERS.[31,33] A comparison of the Raman spectra of R6G on Ag-800 and R6G on Ag nanoparticles (experimental details of the synthesis of the silver nanoparticles was reported earlier[34]) with smooth surfaces and a size of about 73 nm is shown in Figure 8 (B). As expected, Ag-800 exhibited a more than fourfold increase in SERS intensity over the Ag nanoparticles.

A high surface area-to-volume ratio and rich, sharp edges and tips on the surface of a substrate generally benefit SERS properties. Sample Ag-10 shows a weaker signal because of a lower surface area-to-volume ratio. It has been reported that Ag nanoplates with a size of 100–300 nm exhibit a weaker enhancement relative to wires or spheres,[16] and Jana and co-workers also observed that nanoplates with a size above 100 nm produce a weaker signal.[35] How-

ever, although the Ag-400 nanodendrites have higher surface areas, their Raman scattering enhancement is relatively weaker than that of Ag-800. This result could be understood in light of the fact that the Ag-800 nanospheres made up of the primary nanoparticles have some excellent surface features that differ greatly from the other four samples: (i) the nanoscale cavities between the primary nanoparticles on the nanospheres surface are potential "hot" spots for localized near-field enhancement effects,[36,37] and (ii) a large total surface area because of the roughness of the surface of the nanospheres.[4,31,33] Excited by the incident radiation, a collective surface plasmon is trapped between the neighboring nanoscale cavities, thus creating a huge local electric field at these crevices. For example, Xu and coworkers reported that an electric field enhancement of 10^{10} could be achieved between two nanoparticles with 1 nm spacing.[38] According to Pendry's calculations, these local resonant plasmon modes are able to produce an enhancement as large as 10^7 in the Raman intensity of the target molecules adsorbed at these particular crevices.[39] Therefore, it is not surprising to observe that the nanospheres made up of the primary nanoparticles exhibit higher Raman intensity enhancement than the other samples in our present experiment.

As mentioned above, the catalytic activities of metal nanoparticles with different shapes could be evaluated through catalytic processes. As shown in the Figure S2 in the Supporting Information, we can observe a redshift from 313 to 400 nm in the absorption band when $NaBH_4$ is added to a solution of 4-nitrophenol due to generation of 4-nitrophenolate anions. This is observed as an alteration of the color of the solution in a quartz cell from light yellow to yellow-green. Subsequently, the absorption band at 400 nm can be kept for a long time without alteration, which implies that 4-nitrophenolate anions cannot be reduced by aqueous $NaBH_4$. However, when colloidal silver nanomaterials are added to the mixture, an interesting phenomenon is observed, namely, the absorption band at 400 nm quite quickly decreases accompanied by the appearance of new absorption bands at 309 nm, which indicates that 4-aminophenol is formed. This indicates that reduction of 4-nitrophenol by $NaBH_4$ can be activated by colloidal silver nanomaterials.

To evaluate the catalytic activities of the Ag nanomaterials with different shapes, the four samples were added into the reactant solution. Figure 9 (A) shows that the color of the 4-nitrophenolate anions can be faded with time after addition of colloidal Ag-800 (Figure S3 in the Supporting Information shows successive UV/Vis spectra of 4-nitrophenol reduced by $NaBH_4$ with Ag-10, Ag-20, and Ag-400, respectively). As discussed in the experimental details, the redox reaction could be assumed to be a pseudo-first-order kinetic reaction in that the concentration of $NaBH_4$ is constant in the redox reaction. As shown in Figure 9B, the correlation between $\ln(A)$ and reaction time appears linear and a kinetic reaction rate constant can be calculated. As far as Ag-800 is concerned, the kinetic reaction rate is suggested to be $1.27 \times 10^{-2}\ S^{-1}$, which is remarkably higher than that of Ag-400 ($8.53 \times 10^{-3}\ S^{-1}$), Ag-50 ($2.24 \times 10^{-3}\ S^{-1}$), and Ag-10 ($8.92 \times 10^{-4}\ S^{-1}$). It is suggested that catalytic activities of Ag-800 made of the primary nanoparticles are higher than those of the other nanomaterials.

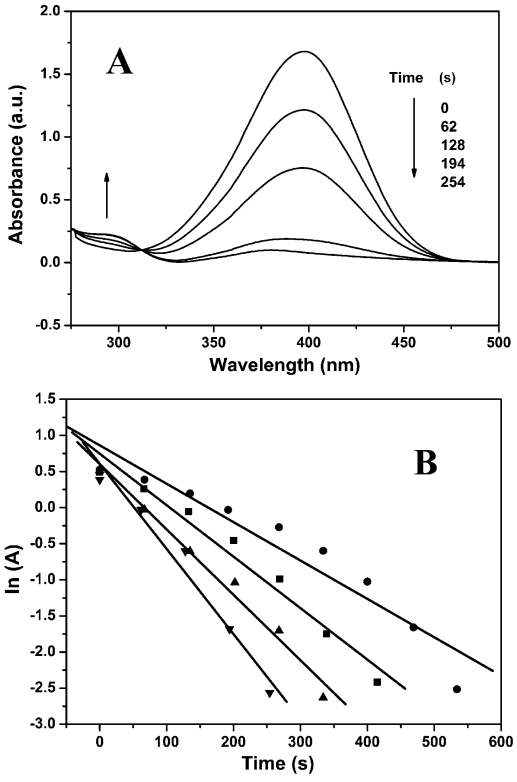

Figure 9. (A) Successive UV/Vis spectra of 4-nitrophenol reduced by $NaBH_4$ with Ag-800. (B) Plot indicating the variation of $\ln(A)$ versus time for the different samples in the reaction: (●) Ag-800, (■) Ag-400, (▲) Ag-50, and (♦) Ag-10.

As is well known, metal nanoparticles can catalyze redox reactions due to their electrochemical current potentials.[40] Therefore, it is reasonable to believe that Ag nanomaterials are electronically conducting solids and can efficiently catalyze some unfeasible redox reactions. As far as the redox reactions of $NaBH_4$ and 4-nitrophenol are concerned, electron transfer between reductant BH_4^- anions and 4-nitrophenolate anions is aided by the surface of silver dendrites. Firstly, 4-nitrophenolate ions are absorbed onto the surface of silver nanomaterials. Then, electrons can be transferred from BH_4^- anions to 4-nitrophenolate anions on the surface of silver nanomaterials and released from the surface of silver nanomaterials. The adsorption of 4-nitrophenolate ions onto the particle surface contributes to the overcoming of the kinetic barrier of the reaction. The relatively large surface area-to-volume ratio of Ag-800 compared to the other Ag nanomaterials (the ratio of relative surface areas of different materials: $A_{Ag\text{-}10}/A_{Ag\text{-}50}/A_{Ag\text{-}400}/A_{Ag\text{-}800}$ = 1:2:10:15; details of calculation shown in the Supporting Information) thus helps to strengthen adsorption of 4-nitrophenolate ions and makes it easier to overcome the kinetic barrier of the redox reaction. Hence, the kinetic reaction rate constant ($1.27 \times 10^{-2}\ S^{-1}$) of catalytic reduction on Ag-800 is larger

than that on the other nanomaterials (8.53×10^{-3}, 2.24×10^{-3}, and 8.92×10^{-4} S^{-1}). The kinetic reaction rate constant of Ag-800 is two times higher than that of Ag nanodendrites (5.19×10^{-3} S^{-1})[23] for the reduction of the 4-nitrophenol when the quantity of Ag nanomaterials was the same as used in the redox reaction, thereby suggesting that the catalytic activity of the as-prepared Ag-800 holds considerable promise for the redox reaction of 4-nitrophenol.

Conclusion

Ag nanomaterials with different shapes can be synthesized by means of a facile approach, that is, $AgNO_3$ reduced by vitamin C in methanol without using any special surfactant. By changing the molar ratio of vitamin C to $AgNO_3$ with a considerable range of about 800, a transition of shape-selective silver nanostructures from nanoplates to nanodendrites and to nanospheres made up of primary nanoparticles can be readily controlled. Furthermore, silver nanomaterials of various shapes can be synthesized depending on the density of the solvent, by using which we can speculate on the shape of the silver nanostructures during the efficient density-assisted self-assembly synthesis. Compared with the other silver nanomaterials presented here, the nanospheres made up of primary nanoparticles showed excellent surface-enhanced effects and catalytic activity that make it another promising candidate for biosensing and use as a catalyst.

Experimental Section

Preparation of Ag Nanomaterials with Different Shapes: Silver nitrate ($AgNO_3$), vitamin C, glycol, isopropyl alcohol, methanol, DMF, acetonitrile, and acetate were all A.R. grade and obtained from Shanghai Reagent Co. All the reagents in the experiment were used as received.

In a typical synthesis of Ag nanomaterials, an aqueous solution of vitamin C (0.6 mL of a 0.1 M solution) was added to methanol (10 mL). Subsequently, an aqueous solution of $AgNO_3$ (1 mL of a 6 mM solution) was added to the solution of vitamin C in methanol. The final concentrations of vitamin C and $AgNO_3$ were 6 mM and 0.6 mM, respectively. The color of the solution changed from colorless to faint yellow within a time span of 10 min, thereby indicating that the Ag nanomaterials were synthesized. The sample is named Ag-10; the numerical values represent the millimolar ratio of vitamin C to $AgNO_3$. To study the effects of the millimolar ratio of vitamin C to $AgNO_3$ on the shape of the Ag nanomaterials, changes to the millimolar ratio were made, and these changes are specified in the Table 1.

Characterization of Ag Nanomaterials with Different Shapes: For field-emission scanning electron microscopy (FESEM) studies, a suspension of Ag was drop-cast on a silicon substrate followed by air drying. The samples were then analyzed with a Sirion 200 field-emission scanning electron microscope operating at an acceleration voltage of 1.0 kV. Before transmission-electron microscopy (TEM) imaging, each resulting Ag nanomaterial colloid (0.01 mL) was drop-cast onto a carbon-coated copper grid and dried at room temperature. TEM was performed with a Hitachi 800 microscope operating at 200 kV. X-ray diffraction (XRD) analyses of the different dried samples, deposited on a microscopic glass slide, were carried out with a Philips X'Pert diffractometer with Cu-K_α radiation (λ = 1.5418 Å) as X-ray source. The absorption of the sample was recorded with a Cintra 10e (GBC, Victoria, Australia) UV/Vis absorption spectrophotometer.

SERS Measurements: For the preparation of SERS substrates, reaction solution (1 mL) was taken out and centrifuged. The precipitate was washed with deionized water three times, and then redispersed in deionized water (100 μL). SERS substrates were prepared by dropping the aqueous solution (25 μL) on a 4×4 mm^2 Si wafer. According to our FESEM observations, the Ag nanomaterials were distributed comparatively homogeneously on the substrates. Then the substrates were immersed in an aqueous solution of rhodamine 6G (R6G) (10 nM) for 1 h. The samples were then taken out, rinsed with deionized water, and dried in air. Raman spectra were measured with a Renishaw 1000 confocal microscopy Raman spectrometer equipped with a CCD detector and a holographic notch filter. Radiation of 514.5 nm from an air–argon ion laser (Spectra-Physics model 163-C4260) was used for excitation. The laser power at the sample position was not more than 2 mW and the laser beam was focused on the sample at a size of about 2 μm. The typical accumulation time used for the study was 1 s. For each sample, we took three SERS spectra in different positions of the substrate and then averaged them.

Catalytic Activity Measurements: A catalytic redox reaction of 4-nitrophenol by silver nanomaterials in aqueous $NaBH_4$ solution can be described in detail. The catalytic redox reaction process was set up in a standard cell with 1 cm path length and 3 mL volume. After $NaBH_4$ (0.1 mL of a 0.3 M solution) had been added to a quartz cell containing 4-nitrophenol (3.4 mL of a 0.1 mM solution) with stirring at 293 K, the color changed from light yellow to yellow-green. Immediately after the addition of silver nanomaterials (40 μL of a 0.5 mM dispersed solution), the absorption spectra were continually recorded with a Shimadzu UV2550 spectrophotometer over a scanning range of 200–500 nm at 293 K. The rate constant of the redox reaction was dependent on the change in absorbance at 400 nm as a function of time.

Supporting Information (see also the footnote on the first page of this article): Includes Figures S1–S3 (FESEM images of the Ag nanomaterials and UV/Vis spectrum of 4-nitrophenol) and calculated details of the relative surface area of different samples.

Acknowledgments

The financial support of this work by the National Science Foundation of China (project nos. 60574095), National Basic Research Program of China (2007CB936603 and 2009CB939902), China Postdoctoral Science Foundation funded project (20070420739) and Hi-Tech Research and Development Program of China (863 Program) (2009AA03Z330) is gratefully acknowledged.

[1] C. X. Zhang, P. Chen, J. Liu, Y. H. Zhang, W. Shen, H. L. Xu, Y. Tang, *Chem. Commun.* **2008**, 3290–3292.
[2] K. Yliniemi, M. Vahvaselka, Y. Van Ingelgem, K. Baert, B. P. Wilson, H. Terryn, K. Kontturi, *J. Mater. Chem.* **2008**, *18*, 199–206.
[3] P. Ahonen, D. J. Schiffrin, J. Paprotny, K. Kontturi, *Phys. Chem. Chem. Phys.* **2007**, *9*, 651–658.
[4] X. M. Qian, S. M. Nie, *Chem. Soc. Rev.* **2008**, *37*, 912–920.
[5] L. L. Sun, Y. H. Song, L. Wang, C. L. Guo, Y. J. Sun, Z. L. Liu, Z. Li, *J. Phys. Chem. C* **2008**, *112*, 1415–1422.

[6] H. Wang, N. J. Halas, *Adv. Mater.* **2008**, *20*, 820–825.
[7] P. S. Kumar, I. Pastoriza-Santos, B. Rodriguez-Gonzalez, F. J. Garcia de Abajo, L. M. Liz-Marzan, *Nanotechnology* **2008**, *19*, 1–5.
[8] S. J. Guo, L. Wang, E. K. Wang, *Chem. Commun.* **2007**, 3163–3165.
[9] P. Zhou, Z. H. Dai, M. Fang, X. H. Huang, J. C. Bao, J. F. Gong, *J. Phys. Chem. C* **2007**, *111*, 12609–12616.
[10] C. L. Nehl, H. W. Liao, J. H. Hafner, *Nano Lett.* **2006**, *6*, 683–688.
[11] V. Polshettiwar, B. Baruwati, R. S. Varma, *ACS Nano* **2009**, *3*, 728–736.
[12] M. N. Nadagouda, R. S. Varma, *Cryst. Growth Des.* **2007**, *7*, 2582–2587.
[13] Y. L. Wang, P. H. Camargo, S. E. Skrabalak, H. C. Gu, Y. N. Xia, *Langmuir* **2008**, *24*, 12042–12046.
[14] A. I. Bhatt, A. Mechler, L. L. Martin, A. M. Bond, *J. Mater. Chem.* **2007**, *17*, 2241–2250.
[15] Y. Sun, Y. N. Xia, *Adv. Mater.* **2003**, *15*, 695–699.
[16] J. T. Zhang, X. L. Li, X. M. Sun, Y. D. Li, *J. Phys. Chem. B* **2005**, *109*, 12544–12548.
[17] J. J. Prywer, *J. Cryst. Growth* **2001**, *224*, 134–144.
[18] Y. Gao, P. Jang, D. F. Liu, H. Y. Yuan, X. Q. Yan, Z. P. Zhou, J. X. Wang, L. Song, L. F. Liu, W. Y. Zhou, G. Wang, C. Y. Wang, S. S. Xie, *J. Phys. Chem. B* **2004**, *108*, 12877–12881.
[19] L. P. Jiang, J. M. Zhu, J. R. Zhang, J. J. Zhu, H. Y. Chen, *Inorg. Chem.* **2004**, *43*, 5877–5883.
[20] K. L. Kelly, E. Coronado, L. L. Zhao, G. C. Schatz, *J. Phys. Chem. B* **2003**, *107*, 668–677.
[21] L. L. He, M. S. Lin, H. Li, N. Kim, *J. Raman Spectrosc.* **2009**, DOI: 10.1002/jrs.2505.
[22] L. H. Lu, A. Kobayashi, K. Tawa, Y. Ozaki, *Chem. Mater.* **2006**, *18*, 4894–4901.
[23] M. H. Rashid, T. K. Mandal, *J. Phys. Chem. C* **2007**, *111*, 16750–16760.
[24] H. T. Zhu, J. X. Wang, G. Y. Xu, *Cryst. Growth Des.* **2009**, *9*, 633–638.
[25] H. T. Zhu, C. Y. Zhang, Y. S. Yin, *J. Cryst. Growth* **2004**, *270*, 722–728.
[26] N. N. Mallikarjuna, V. Polshettiwar, R. S. Varma, *J. Mater. Chem.* **2009**, *19*, 2026–2031.
[27] C. Burda, X. Chen, R. Narayanan, M. A. El-Sayed, *Chem. Rev.* **2005**, *105*, 1025–1102.
[28] X. S. Fang, C. H. Ye, X. S. Peng, Y. H. Wang, Y. C. Wu, L. D. Zhang, *J. Mater. Chem.* **2003**, *13*, 3040–3043.
[29] J. M. Petroski, Z. L. Wang, T. C. Green, M. A. El-Sayed, *J. Phys. Chem. B* **1998**, *102*, 3316–3320.
[30] M. N. Nadagouda, R. S. Varma, *Green Chem.* **2006**, *8*, 516–518.
[31] Y. Yang, S. Matsubara, L. M. Xiong, T. Hayakawa, M. Nogami, *J. Phys. Chem. C* **2007**, *111*, 9095–9104.
[32] Y. Lu, G. L. Liu, L. P. Lee, *Nano Lett.* **2005**, *5*, 5–9.
[33] J. Zhao, A. O. Pinchuk, J. M. McMahon, S. Z. Li, L. K. Ausman, A. L. Atkinson, G. C. Schata, *Acc. Chem. Res.* **2008**, *41*, 1710–1720.
[34] P. C. Lee, D. Meisel, *J. Phys. Chem.* **1982**, *86*, 3391–3395.
[35] N. R. Jana, T. Pal, *Adv. Mater.* **2007**, *19*, 1761–1765.
[36] W. Y. Li, P. H. C. Camargo, X. M. Lu, Y. N. Xia, *Nano Lett.* **2009**, *9*, 485–490.
[37] X. S. Shen, G. Z. Wang, X. Hong, W. Zhu, *Phys. Chem. Chem. Phys.* **2009**, *11*, 7450–7454.
[38] H. X. Xu, E. J. Bjerneld, M. Kall, L. Borjesson, *Phys. Rev. Lett.* **1999**, *83*, 4357–4360.
[39] F. J. Garcia-Vidal, J. B. Pendry, *Phys. Rev. Lett.* **1996**, *77*, 1163–1166.
[40] D. S. Miller, A. J. Bard, G. Mclendom, J. Ferguson, *J. Am. Chem. Soc.* **1981**, *103*, 5336–5341.

Received: November 18, 2009
Published Online: March 17, 2010

